CORRELATIONS IN LARGE p_T PROCESSES IN PARTON MODELS

By W. Furmański and J. Wosiek

Institute of Physics, Jagellonian University, Cracow*

(Received March 10, 1977)

We calculate the two-particle distribution and the associated multiplicity for large p_T region in the framework of the parton models. We find that it is possible to construct a model beeing able to fit quite well a large amount of data on the two-particle level. The model should possess the following properties: a) the hard scattering cross-section should be independent of energy at fixed p_T, b) both quasi-exclusive (single-jet) and inclusive (double-jet) components must be present with the cross-section for the double-jet process at least one order of magnitude larger than that for the single-jet process, c) the mean transverse momentum in the jet fragmentation should be of the order of 630 MeV, d) the jet structure function should be damped like $(1-x)^2$ for $x \to 1$.

1. Introduction

The general picture of hadron production, in the large p_T region, resulting from experimental research at ISR indicates that the hard scattering model may provide the correct dynamical description of hadronic interactions in this region. The most rigorous test for the validity of the underlaying parton dynamics — presence of jets in the final state — seems to be confirmed by recent SFM measurements [1].

However, this success of jet models is up to now only of qualitative character: none of important parameters, like widths, slopes etc. are successfully predicted or explained by the jet dynamics. The reason is that the description of the final state in the "naive" parton model with zero width jets is too much simplified to give realistic quantitative results. If one uses the standard form for the inclusive distribution of particles produced by the jet fragmentation

$$\left(\frac{\frac{dN}{d^3p_1}}{E_1}\right)_{J_1 \to 1+X} = \frac{1}{\pi}\,\delta(\hat{p}^2_{T1|J_1})G_{1|J_1}(\hat{x}_1)\hat{x}_1 \tag{1.1}$$

* Address: Instytut Fizyki UJ, Reymonta 4, 30-059 Kraków, Poland.

(where $\hat{p}_{T1|J_1}$ is the transverse momentum of $\hat{\vec{p}}_1$ relative to the jet J_1 axis, $\hat{x}_1$ is the longitudinal fraction of the jet momentum taken by $\hat{\vec{p}}_1$ and $G_{1|J_1}(\hat{x}_1)$ is the structure function for the jet fragmentation) then the resulting final state configuration is exactly planar. If one calculates P_{out} or azimuthal distributions one obtains simply δ functions while the experimental shapes are quite broad.

There is also some indirect evidence coming from the momentum dependence observed experimentally, that the scale-invariant formula (1.1) is not able to reproduce the data. For example, it was reported by the ACHM Collaboration [2] that the two-particle inclusive distribution for two large p_T particles in the same direction can be described by the same functional dependence as the one particle distribution, i. e.

$$\left.\frac{d\sigma}{\frac{d^3p_1}{E_1}\frac{d^3p_2}{E_2}}\right|_{\varphi\approx 0,|y_1-y_2|\approx 0} = \frac{c_{12}}{(p_{T1}+p_{T2})^N} e^{-B(x_{T1}+x_{T2})}, \tag{1.2}$$

while

$$\frac{d\sigma}{\frac{d^3p_1}{E_1}} = \frac{c_1}{p_{T1}^N} e^{-Bx_{T1}}. \tag{1.3}$$

Without detailed calculations one can expect that the jet model with the scale-invariant fragmentation spectrum will be in trouble with this observation. The reason is pure dimensional: the distributions (1.2) and (1.3) have different dimensions and thus it is impossible to obtain the same power N in both formulas if (1.1) contains no dimensional parameters. Some additional factors like $\frac{1}{s}$, $\frac{1}{p_{T1}p_{T2}}$, $\frac{1}{(p_{T1}+p_{T2})^2}$ etc. must appear in Eq. (1.2), restoring the correct dimension but spoiling the form (1.2), observed experimentally.

Another piece of the data, which indicates the relevance of some dimensional parameter in the final state is the associated multiplicity of charged particles observed exactly opposite in azimuth to the triggered large p_T particle. It grows nearly linearly with p_T, i. e.

$$\left.\frac{dN^{opp}_{2(1)}}{d\varphi dy_2}\right|_{\varphi\approx\pi,y_2\approx 0} \sim \alpha_0+\alpha_1 p_{T1}, \tag{1.4}$$

and we have the next dimensional trouble of the model with the scale-invariant decay spectrum: α_1 must have dimension since the left-hand side is dimensionless. Since the masses of the particles are generally believed to be irrelevant in the large p_T region, the realistic jet fragmentation spectrum must contain some dimensional parameter, from which α_1 could be constructed.

In the present paper we calculate the two-particle distribution using the finite $\hat{p}_{T1|J_1}$ distribution. As a natural generalization of (1.1) we choose

$$\left(\frac{\frac{dN}{d^3p_1}}{E_1}\right)_{J_1\to 1+X} = \frac{A}{\pi} e^{-Ap_{T1|J1}{}^2}\hat{x}_1 G_{1|J_1}(\hat{x}_1), \tag{1.5}$$

where

$$G_{1|J_1}(\hat{x}_1) \equiv \frac{1}{\hat{x}_1} F_{1|J_1}(\hat{x}_1) = \frac{n_{1|J_1}}{\hat{x}_1}(1-\hat{x}_1)^{g_{1|J_1}}. \tag{1.6}$$

Now all the widths in resulting angular distributions are finite and controlled by the value of A. In particular, in the limit $A \to \infty$ we recover the zero width formula (1.1).

To get definite predictions in the parton model one has to choose some formula for the hard scattering cross-section. Instead of limiting ourselves to any particular model, we try to perform a model independent analysis, i. e. we parametrize so the hard scattering cross-section as to include the broad class of models, calculate the yields and finally look for what values of the parameters (i. e. for what model) the best fit to the data can be obtained. Thus the result of our analysis is the collection of constraints which must be satisfied by the model to fit succesfully the data. We do not discuss here the problem how far these constraints are indeed obeyed by the up to now proposed parton models.

The paper is organized as follows: in Chapter 2 we present our parametrization of the hard scattering cross-section and calculate the two-particle distribution. Comparison of the resulting formulas with the experiment is presented in Chapter 3 (opposite side correlations) and in Chapter 4 (same side correlations). A short summary can be found in Chapter 5. Some technical details concerning the calculation of the integrals appearing in the parton model formulas are collected in the Appendix. The more detailed description of the method of integration we use can be found in Ref. [9].

2. Calculation of the two-particle distribution

The notation used in this paper is exactly the same as in Ref. [9]: constituents c_1c_2 from incoming protons A, B scatter elastically into two jets J_1, J_2, which in turn "fragment" into detected particles 1, 2. Variables used during the calculation are defined in Fig. 1 (quantities with $\wedge$ refer to the c_1c_2 CM frame, without $\wedge$ to the AB CM frame).

The hard scattering cross-section can be parametrized as follows: from the dimensional analysis which is generally assumed to work in the fixed angle region $s, t \to \infty$, t/s fixed one has

$$\frac{d\sigma_H}{d\hat{t}} = \frac{c_0}{\hat{s}^n} f(\hat{t}/\hat{s}). \tag{2.1}$$

Now, since the left-right symmetry must be obeyed (see [9]) the inclusive yield depends to a good approximation only on the symmetrized cross-section

$$\left(\frac{d\sigma_H}{d\hat{t}}\right)_{sym} = \frac{c_0}{\hat{s}^n}[f(\hat{t}/\hat{s})+f(\hat{u}/\hat{s})] \tag{2.2}$$

what can be written as

$$\left(\frac{d\sigma_H}{d\hat{t}}\right)_{sym} = \frac{c_0}{\hat{s}^n} h(\lambda) = \frac{c_0}{(4\hat{p}_T^2)^n} H(\lambda), \tag{2.3}$$

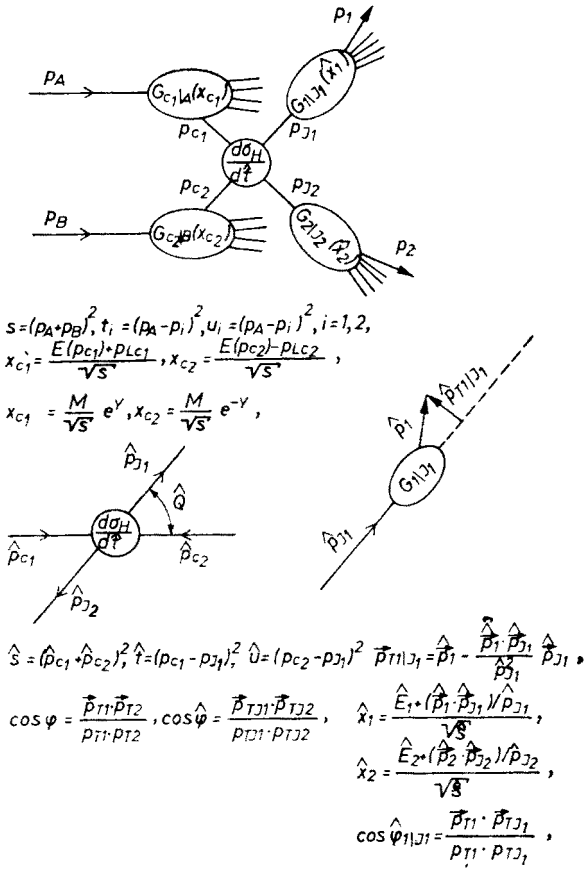

Fig. 1. Definition of the variables used in text

where

$$\lambda = \hat{s}^2/(4\hat{t}\hat{u}) = \cosh^2\hat{y} = 1/\sin^2\hat{\theta},\ H(\lambda) = h(\lambda)/\lambda^n.$$

Since $H(\lambda)$ decreases for large λ (or at least remains constant) due to the factor $1/\lambda^n$ in all up to now proposed hard scattering models, we can write approximately

$$\left(\frac{d\sigma_H}{d\hat{t}}\right)_{\text{sym}} = \frac{c_0 H(1)}{(4\hat{p}_T^2)^n}\, e^{-\alpha\hat{y}^2}. \tag{2.4}$$

Formula (2.4) presents the parametrization we use in the rest of this paper.

The general formula for the two-particle distribution in the parton model reads:

$$\left(\frac{d\sigma}{\frac{d^3p_1}{E_1}\frac{d^3p_2}{E_2}}\right)_{AB\to 1+2+X} = \int dx_{c_1} G_{c_1|A}(x_{c_1}) \int dx_{c_2} G_{c_2|B}(x_{c_2}) \left(\frac{d\sigma}{\frac{d^3p_1}{E_1}\frac{d^3p_2}{E_2}}\right)_{c_1c_2\to 1+2+X}$$

$$+(A \leftrightarrow B,\ J_1 \leftrightarrow J_2) \tag{2.5}$$

where for the structure functions we assume the standard form

$$G_{c_1|A}(x_{c_1}) = \frac{n_{c_1|A}}{x_{c_1}}(1-x_{c_1})^{g_{c_1|A}}, \qquad G_{c_2|B}(x_{c_2}) = \frac{n_{c_2|B}}{x_{c_2}}(1-x_{c_2})^{g_{c_2|B}} \tag{2.6}$$

(transverse motion of constituents c_1, c_2 is neglected).

It is convenient to discuss separately the cases when the particles 1, 2 are produced on the same side: $-\frac{\pi}{2} < \varphi < \frac{\pi}{2}$ (i. e. they come from the same jet) and on the opposite sides: $\frac{\pi}{2} < \varphi < \frac{3}{2}\pi$ (i. e. they come from two different jets).

2.1. Two-particle distribution for the opposite side

We have

$$\left(\frac{d\sigma}{\frac{d^3p_1}{E_1}\frac{d^3p_2}{E_2}}\right)_{c_1c_2\to 1+2+X} = \int \frac{d^3p_{J_1}}{E_{J_1}}\frac{d^3p_{J_2}}{E_{J_2}}\left(\frac{d\sigma}{\frac{d^3p_{J_1}}{E_{J_1}}\frac{d^3p_{J_2}}{E_{J_2}}}\right)_{c_1c_2\to J_1J_2}\left(\frac{dN}{\frac{d^3p_1}{E_1}}\right)_{J_1\to 1+X}\left(\frac{dN}{\frac{d^3p_2}{E_2}}\right)_{J_2\to 2+X} \tag{2.1.1}$$

where $\left(\frac{dN}{\frac{d^3p_i}{E_i}}\right)_{J_i\to i+X}$, $i = 1, 2$, are given by (1.5) and

$$\left(\frac{d\sigma}{\frac{d^3p_{J_1}}{E_{J_1}}\frac{d^3p_{J_2}}{E_{J_2}}}\right)_{c_1c_2\to J_1J_2} = \frac{\hat{s}}{\pi}\frac{d\sigma_H}{d\hat{t}}\delta(\hat{s}+\hat{t}+\hat{u})\hat{E}_{J_2}\delta^3(\hat{\vec{p}}_{J_1}-\hat{\vec{p}}_{J_2}). \tag{2.1.2}$$

Using the parametrization (2.4) for the hard scattering cross-section integrals in (2.1.1) and (2.1.2) can be performed by means of the saddle point method. The detailed calculation can be found in the Appendix, where also the resulting formulas in its most general form are collected.

Here we present only the quasi-exclusive (single-jet) contribution which is found to be responsible for the leading part of the opposite side correlations (see Section 2.3):

$$\left(\frac{d\sigma}{\frac{d^3p_1}{E_1}\frac{d^3p_2}{E_2}}\right)^{\text{opp}}_{AB\to 1+2+X} = \frac{c_{J_1}}{p_{T1}^N}e^{-B(x_{T1},y_1)x_{T1}}\frac{1}{m_{T2}^2}F_{2|J_2}\left(\frac{p_{T2}}{p_{T1}}\right) \times \frac{\exp\left[-\left(\frac{\sin\varphi}{\Delta\varphi}\right)^2\right]}{\sqrt{\pi}\,\Delta\varphi}\frac{\exp\left[-\left(\frac{y_2-y_2^{\max}(x_{T1},y_1)}{\Delta y_2}\right)^2\right]}{\sqrt{\pi}\,\Delta y_2} \times\left[\theta(x_{T1}-x_{T2})+O\left(\left(\frac{x_{T1}}{x_{T2}}\right)^{N-2}\right)\theta(x_{T2}-x_{T1})\right], \tag{2.1.3}$$

where $N = 2n$,

$$B(x_{T1}, 0) = B(0, 0) \equiv B = g_{c_1|A} + g_{c_2|B}, \tag{2.1.4}$$

$$B(x_{T1}, y_1) = B\left[\frac{Bx_{T1}}{Bx_{T1}+\alpha}\,\tfrac{1}{2}\,(1+\cosh y_1) + \frac{\alpha}{Bx_{T1}+\alpha}\cosh y_1\right], \tag{2.1.5}$$

$$c_{J_1} = \frac{c_0 H(1)}{2^N}\,\frac{n_{c_1|A} n_{c_2|B}}{\sqrt{Bx_{T1}+\alpha}}, \tag{2.1.6}$$

$$\Delta\varphi = \frac{1}{\sqrt{A}\,p_{T2}}, \quad \Delta y_2 = \frac{2}{\sqrt{Bx_{T1}+\alpha}}\sqrt{\frac{4Ap_{T2}^2 + Bx_{T1}+\alpha}{4Ap_{T2}^2}}, \tag{2.1.7,8}$$

$$y_2^{\max}(x_{T1}, y_1) = \frac{\alpha}{Bx_{T1}+\alpha}\,y_1 + \frac{Bx_{T1}}{Bx_{T1}+\alpha}\,\bar{y}_1, \tag{2.1.9}$$

$$\bar{y}_1 = \tfrac{1}{2}\ln\frac{1-\frac{1}{2}x_{T1}e^{y_1}}{1-\frac{1}{2}x_{T1}e^{-y_1}}.$$

(We do not display explicitly the second term in (2.1.3) since it is strongly damped relatively to the first one by the factor $\left(\frac{x_{T1}}{x_{T2}}\right)^{N-2}$ and can be neglected in the rough numerical analysis we perform in this paper. The complete formula can be found in the Appendix). The first term in (2.1.3) is nothing but the one-particle distribution (see [9])

$$\left(\frac{\frac{d\sigma}{d^3p_1}}{E_1}\right)_{AB\to 1+X} = \frac{c_{J_1}}{p_{T1}^N}\,e^{-B(x_{T1},y_1)x_{T1}} + (J_1 \leftrightarrow J_2), \tag{2.1.10}$$

and thus the associated multiplicity away is given by

$$\frac{\frac{dN_{2(1)}^{\text{opp}}}{d^3p_2}}{E_2} = \left(\frac{\frac{d\sigma}{d^3p_1\,d^3p_2}}{E_1\,E_2}\right)_{AB\to 1+2+X} \Bigg/ \left(\frac{\frac{d\sigma}{d^3p_1}}{E_1}\right)_{AB\to 1+X}$$

$$= \frac{1}{m_{T2}^2}\,F_{2|J_2}\left(\frac{p_{T2}}{p_{T1}}\right)\frac{\exp\left[-\left(\frac{\sin\varphi}{\Delta\varphi}\right)^2\right]}{\sqrt{\pi}\,\Delta\varphi}\,\frac{\exp\left[-\left(\frac{y_2 - y_2^{\max}(x_{T1}, y_1)}{\Delta y_2}\right)\right]}{\sqrt{\pi}\,\Delta y_2}$$

$$\times\left[\theta(x_{T1}-x_{T2}) + O\left(\left(\frac{x_{T1}}{x_{T2}}\right)^{N-2}\right)\theta(x_{T2}-x_{T1})\right]. \tag{2.1.11}$$

2.2. Two-particle distribution for the same side

We have now

$$\left(\frac{d\sigma}{\frac{d^3p_1}{E_1}\frac{d^3p_2}{E_2}}\right)^{\text{same}}_{c_1c_2\to 1+2+X} = \int \frac{d^3p_{J_1}}{E_{J_1}}\frac{d^3p_{J_2}}{E_{J_2}}\left(\frac{d\sigma}{\frac{d^3p_{J_1}}{E_{J_1}}\frac{d^3p_{J_2}}{E_{J_2}}}\right)_{c_1c_2\to J_1J_2}\left(\frac{dN}{\frac{d^3p_1}{E_1}\frac{d^3p_2}{E_2}}\right)_{J_1\to 1+2+X} \tag{2.2.1}$$

Where $d\sigma_{c_1c_2\to J_1J_2}$ is given by (2.1.2).

The simplest form for $dN_{J_1\to 1+2+X}$, which reflects only the long range phase space correlations is

$$\left(\frac{dN}{\frac{d^3p_1}{E_1}\frac{d^3p_2}{E_2}}\right)_{J_1\to 1+2+X} = \frac{A}{\pi}e^{-A\hat{p}_{T1|J_1}^2}\frac{A}{\pi}e^{-A\hat{p}_{T2|J_1}^2}\hat{x}_1\hat{x}_2G_{12|J_1}(\hat{x}_1,\hat{x}_2) \tag{2.2.2}$$

with

$$G_{12|J_1}(\hat{x}_1,\hat{x}_2) = \frac{1}{\hat{x}_1\hat{x}_2}F_{12|J_1}(\hat{x}_1+\hat{x}_2),$$

$$F_{12|J_1}(\hat{x}_{12}) = n_{12|J_1}(1-\hat{x}_{12})^{g_{12|J_1}}. \tag{2.2.3}$$

The calculation of the integrals in (2.1.1) and (2.2.1) can be found in the Appendix and the final result reads:

$$\left(\frac{d\sigma}{\frac{d^3p_1}{E_1}\frac{d^3p_2}{E_2}}\right)^{\text{same}}_{AB\to 1+2+X} = \frac{A}{\pi}\frac{c_{12|J_1}}{(p_{T1}+p_{T2})^N}e^{-B_{12}(x_{T12},y_{12})x_{T12}}$$

$$\times\frac{(p_{T1}+p_{T2})^2}{p_{T1}^2+p_{T2}^2}e^{-A\frac{p_{T1}^2p_{T2}^2}{p_{T1}^2+p_{T2}^2}\sin^2\varphi}e^{-A\frac{p_{T1}^2p_{T2}^2}{p_{T1}^2+p_{T2}^2}(y_1-y_2)^2}, \tag{2.2.4}$$

where $x_{T12} = x_{T1}+x_{T2}$, $y_{12} = \frac{1}{2}(y_1+y_2)$.

$$B_{12}(x_{T12},0) = B_{12}(0,0) \equiv B_{12} = \frac{1}{\langle\hat{x}_{12}\rangle}(g_{c_1|A}+g_{c_2|B}), \quad \langle\hat{x}_{12}\rangle = \frac{N-3}{N-2+g_{12|J_1}},$$

$$B_{12}(x_{T12},y_{12}) = B_{12}\left[\frac{B_{12}x_{T12}}{B_{12}x_{T12}+\alpha}\tfrac{1}{2}(1+\cosh y_{12})+\frac{\alpha}{B_{12}x_{T12}+\alpha}\cosh y_{12}\right],$$

$$c_{12|J_1} = \langle\hat{x}_{12}^{N-2}\rangle c_{J_1}, \quad \langle\hat{x}_2^{N-2}\rangle = \int_0^1 d\hat{x}_{12}\hat{x}_{12}^{N-3}F_{12|J_1}(\hat{x}_{12}),$$

$$c_{J_1} = \frac{c_0}{2^N}H(1)n_{c_1|A}n_{c_2|B}\frac{1}{\sqrt{B_{12}x_{T12}+\alpha}}, \quad N = 2n.$$

2.3. Relative normalization of various subprocesses

Before we start to compare our results with the experiment we have to decide which elementary subprocesses $c_1 c_2 \to J_1 J_2$ give the leading contribution to the total yield.

The first well-known constraint is provided by the quark counting rules for the power N: $\frac{1}{2}N = N_q - 2$, where N_q is the number of quarks in the hard scattering. To obtain the correct value of $N \approx 8$ for the meson production in ISR (we limit ourselves to this process) all processes with $N_q < 6$ must be excluded and the processes with $N_q > 6$ can be neglected to a first approximation. What remains are the processes like: $Mq \to Mq$, $M\overline{M} \to q\bar{q}$, $q\bar{q} \to M\overline{M}$, $q(qq) \to q(qq)$ with all possible jet fragmentations in the final state.

The next important restriction can be expressed as follows: if for a given subprocess a quasi-exclusive limit exists (i. e. the detected particle is just the jet particle) then all the inclusive versions of this subprocesses can be neglected relative to the quasi-exclusive component (e. g. $Mq \to M^*(\to M+X)q$ can be neglected relative to $Mq \to Mq$ with $M = 1 = J_1$. Note also, that for $M\overline{M} \to q\bar{q}$, $q(qq) \to q(qq)$ the quasi-exclusive limit does not exist — quarks and diquarks must fragment. This constraint follows from the following relation between the normalization constants [9]:

$$c_{1|J_1} = \langle \hat{x}_1^{N-2} \rangle c_{J_1}, \tag{2.3.1}$$

where c_{J_1} is the normalization constant for the quasi-exclusive process $c_1 c_2 \to J_1(=1)J_2$ and $c_{1|J_1}$ the one for its inclusive version $c_1 c_2 \to J_1(\to 1+X)J_2$ and

$$\langle \hat{x}_2^{N-2} \rangle = \int_0^2 d\hat{x}_1 \hat{x}_1^{N-2} G_{1|J_1}(\hat{x}_1) = n_{1|J_1} \frac{(g_{1|J_1})!(N-3)!}{(N-2+g_{1|J_1})!}. \tag{2.3.2}$$

From the phase space sum rule

$$\sum_1 \int_0^1 \hat{x}_1 G_{1|J_1}(\hat{x}_1) d\hat{x}_1 = 1 \tag{2.3.2}$$

we find easily the bound $n_{1|J_1} \leqslant g_{1|J_1}+1$ and thus

$$\langle \hat{x}_1^{N-2} \rangle \leqslant \frac{(g_{1|J_1}+1)!(N-3)!}{(N-2+g_{1|J_1})!}. \tag{2.3.4}$$

For $N = 8$ we obtain from (2.3.4)

$$\langle \hat{x}_1^6 \rangle \leqslant \tfrac{1}{21} \text{ for } g_{1|J_1} = 1, \quad \langle \hat{x}_1^6 \rangle \leqslant \tfrac{1}{56} \text{ for } g_{1|J_1} = 2,$$
$$\langle \hat{x}_1^6 \rangle \leqslant \tfrac{1}{126} \text{ for } g_{1|J_1} = 3 \text{ etc.} \tag{2.3.5}$$

The intuitive origin of this constraint is quite obvious: to produce the large p_T particle as a child of some parent jet, the hard scattering must occur at larger energy $\hat{s}$ than the one for the direct jet production and thus it is more supressed by the factor $\langle \hat{x}_1^{N-2} \rangle$ in (2.3.1). In the following we will use the names: single-jet process (double-jet process) for the process which have (do not have) the quasi-exclusive limit.

It follows from the above considerations, that if a single jet process and a double-jet process have comparable hard scattering cross-sections then the contribution from the double-jet process to the total inclusive yield can be neglected (just due to the extra factor $\langle \hat{x}_{21}^{N-2} \rangle$ in (2.3.1)).

The guess that all hard scattering cross-sections with the fixed number of external quark legs (i. e. with fixed N) are of the same order looks reasonable as a starting point to our numerical analysis. But if it is indeed the case, then all the double jet processes can be described by quasi-exclusive processes only. It is just what we assume as a starting point.

3. Opposite side correlations — comparison with experiment

Formula (2.1.3) which we use to describe the opposite side correlations data depends on the following parameters: B, α, N, A, $n_{2|J_2}$, $g_{2|J_2}$. Parameters B, α, N are fixed by single-particle distribution: for the meson production we have $N \approx 8$, $B \approx 13$ for π^0, $B \approx 15$ for $\pi^{\pm}$. In Ref. [9] we have found that to reproduce the weak rapidity dependence of the one-particle distribution one has to take $\alpha = 0$ i. e. to assume that the hard scattering does not depend on angle at fixed p_T. Thus α is also fixed and we find further that the constraint $\alpha = 0$ appears to be even much stronger on the two-particle level.

In the measurements of the associated multiplicities one usually sums over all charged secondaries. It is reasonable to assume that the charged particles take 2/3 of the total yield coming from the jet fragmentation. Then the constant $n_{ch|J_2}$ can be determined from the phase space sum rule

$$\sum_{\substack{2 \\ \text{charged}}} \int_0^1 d\hat{x}_2 \hat{x}_2 G_{2|J_2}(\hat{x}_2) \approx \tfrac{2}{3} . \tag{3.1}$$

Since the leading contribution is given by the structure function with the lowest value of $g_{2|J_2}$, we can neglect all decays which are more damped in $\hat{x}_2$ and we find

$$n_{ch|J_2} = \sum_{\substack{2 \\ \text{charged}}} n_{2|J_2} = \tfrac{2}{3}(g_{2|J_2}+1). \tag{3.2}$$

Thus we have only two free parameters A and $g_{2|J_2}$ which must be fited.

3.1. P_{out} distribution

The angular distributions given by the formula (2.1.3) depend essentially on the value of slope A in the jet fragmentation formula. The best place to fit A is the P_{out} distribution, measured by the SFM group [1]. Using the variables $P_{out} = p_{T2} \sin \varphi$, $P_{2x} = p_{T2} \cos \varphi$, $x_E = \dfrac{P_{2x}}{P_{1x}} \approx \dfrac{p_{T2}}{p_{T1}}$, proposed in [1] the formula (2.1.3) can be rewritten for $P_{2x} \gg P_{out}$, $p_{T1} < P_{2x}$ as follows:

$$\frac{dN_{2(1)}^{opp}}{dP_{out} dP_{2x} dy_2} \approx e^{-AP_{out}^2} F(p_{2x}, x_E, y_2). \tag{3.1.1}$$

Thus we obtain the factorisation in the variables P_{out} and P_{2x}, x_E, y_2, reported in [1] and observe, that the slope of the P_{out} distribution measures exactly the slope A in the jet fragmentation spectrum. We find from Fig. 2 where the fit to the SFM data is presented, that the Gaussian shape (3.1.1) reproduces the data rather well for $A = 2$. It corresponds to the mean transverse momentum $\langle p_{T2|J_2} \rangle$ relative to the jet axis

$$\langle \hat{p}_{T2|J_2} \rangle = \tfrac{1}{2}\sqrt{\frac{\pi}{A}} = 0.63 \text{ GeV}/c. \tag{3.1.2}$$

Thus we obtain the value which is remarkably larger than the typical hadronic transverse momentum $\langle p_T \rangle \sim 0.35$ GeV.

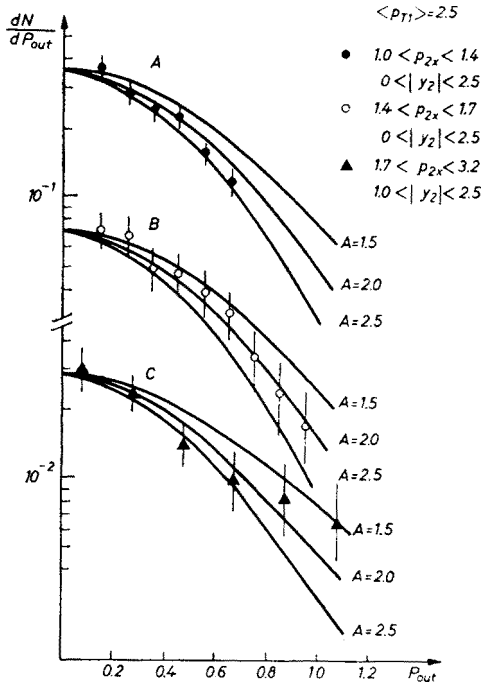

Fig. 2. Fit of the formula (3.1.1) (plots A, B) and (3.1.3) (plot C) to the P_{out} distribution (SFM data from Ref. [1])

For $P_{2x} > p_{T1}$ the second part of (2.1.11) should be used (see Appendix) and we find then

$$\frac{dN^{\text{opp}}_{2(1)}}{dP_{\text{out}} dP_{2x} dy_2} \approx e^{-A \frac{p_{T1}^2}{p_{2x}^2 + P_{\text{out}}^2} P_{\text{out}}^2} F(p_{2x}, x_E, y_2). \tag{3.1.3}$$

Thus we expect that for $P_{2x} > p_{T1}$ the P_{out} distribution should become broader with the slope A_{eff}

$$A_{\text{eff}} \approx A \left(\frac{p_{T1}}{p_{2x}} \right)^2. \tag{3.1.4}$$

This effect seems to be indeed present in the data (see the plot C on Fig. 2, where the slope is really smaller).

The physical meaning of this broadening is the following: for $p_{T1} > P_{2x}$ the configuration measured in the one presented in Fig. 3: particle 1 is the jet particle, particle 2 comes from the J_2 decay and its P_{out} is determined by the slope A. For $P_{2x} > p_{T1}$ the inverse

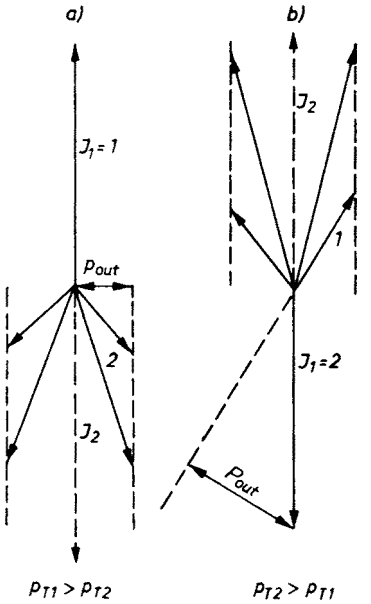

Fig. 3. Pictoral explanation of the broadening of the P_{out} distribution in the quasi-exclusive component for $P_{2x} > p_{T1}$. In Fig. 3a particle 1 is the jet J_1 particle and P_{out} distribution is determined by the slope A. In Fig. 3b particle 1 comes from the jet J_2 and the P_{out} distribution is broader

configuration is detected: the particle 1 is now the jet J_2 fragment and the particle 2 is the jet particle. The mean P_{out} grows, it starts to depend on momenta and, as seen from Fig. 3, formula (3.1.4) can be obtained from simple geometrical considerations.

If further experiments confirm the P_{2x} and p_{T1} dependence of A_{eff} given by (3.1.4), it will be the strong support to our guess that the quasi-exclusive component dominates in the opposite side correlations. Note that for the double-jet process the point $p_{T1} = P_{2x}$ is not market out in any way and thus no essential changes in P_{out} distribution are expected in coming from the region $p_{T1} > P_{2x}$ to $p_{T1} < P_{2x}$.

3.2. x_E distribution

The best place to study the jet structure function is the x_E distribution, measured by SFM group [1]. For fast fragments of the jet we have $x_E \approx \dfrac{p_{T2}}{p_{T1}}$ and intergrating (2.1.11) over angles we find

$$\frac{dN^{opp}_{ch(1)}}{dx_E} \approx \tfrac{2}{3}(g_{2|J_2}+1)\frac{1}{x_E}(1-x_E)^{g_{2|J_2}}\theta(1-x_E). \tag{3.2.1}$$

Thus we expect that the x_E distribution vanish for $x_E > 1$ (in a more rigorous numerical analysis one should take also into account the inverse contribution which would introduce some smearing of the x_E distribution around $x_E = 1$). On the other hand, in the double-jet process the point $x_E = 1$ is by no means marked out and the resulting x_E distribution does not vanish for $x_E = 1$.

As seen from Fig. 4, dN/dx_E is indeed strongly damped for $x_E > 1$ and it provides the next evidence for the dominance of the quasi-exclusive component in the opposite side correlations.

We find from Fig. 4 that the best fit can be obtained for $g_{2|J_2} = 2$. This value seems to be rather reasonable in view of parton model counting rules, where $g_{2|J_2} = 2m_{2|J_2} - 1$,

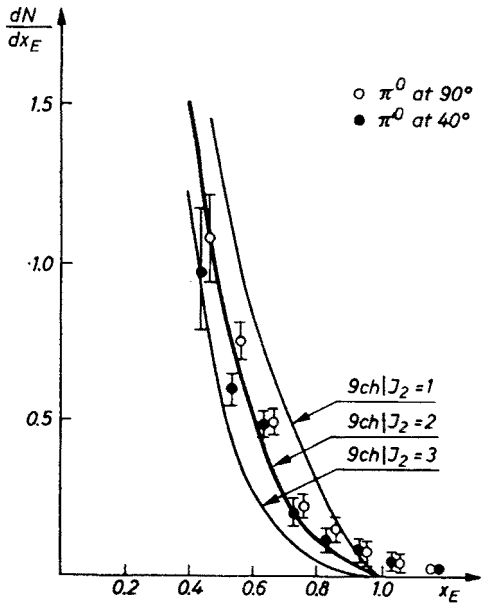

Fig. 4. Fit of the formula (3.2.1) to the x_E distribution (SFM data from Ref. [1])

$m_{2|J_2}$ beeing the minimal number of quarks which must be slowed down to produce the fast fragment 2 from the jet J_2. For simplest jets (quark, diquark) we find for meson production

$$g_{M|q} = 1, \quad g_{M|(qq)} = 3.$$

Thus one can try to understand the experimental value $g_{2|J_2} = 2$ as a result of some mixture of quark and diquark jets.

3.3. y_2 distribution

It was reported first by PSB-Collaboration and then by DILR, ACHM and SFM groups [3, 4, 5, 1, 6] that one observes on the opposite side to the large p_T trigger a broad enhancement on the rapidity axis with the width of order of 4 units. The shape of the

bump depends rather weakly on the momentum of the associated particles (see Fig. 5, where the SFM data for $y_1 = 0$ are presented). The position of the maximum $y_2^{\max}$ is only weakly correlated with the rapidity y_1 of the trigger. It can be observed in Fig. 6 where we have plotted $y_2^{\max}$ as a function of y_1. Some weak back-to-back effect is observed for

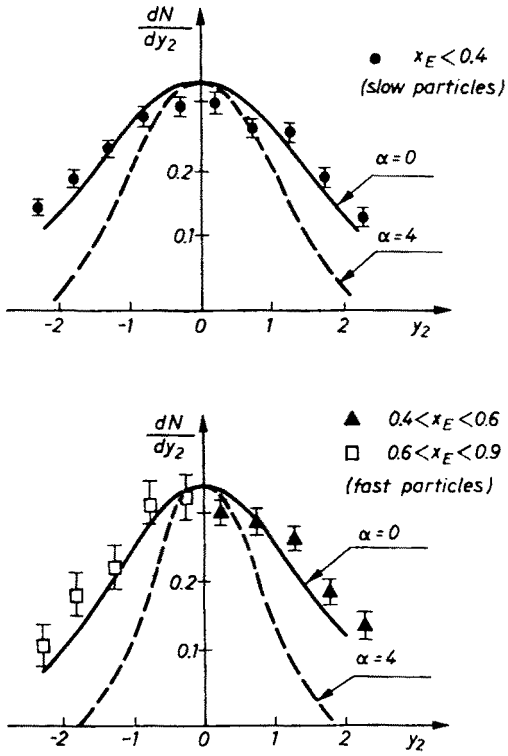

Fig. 5. y_2 distribution (away) for $y_1 = 0$, $\langle p_{T1} \rangle = 2.5$ GeV/c for various P_{2x}. Solid (dashed) line is the prediction of the model for $\alpha = 0$ ($\alpha = 4$) (Formula (3.3.1)). SFM data from Ref. [1]

small y_1 and only for pion triggers, a weak anti-back-to-back effect seems to develop for larger values of y_1. However, the general trend on the bump is to stay at $y_2 = 0$ irrespectively of the rapidity of the large p_T particle.

Various parton models were found to be in trouble with the explanation of this peculiar rapidity distribution and therefore our, to a large extend, model independent considerations seem to be especially useful in this point. From the formula (2.1.11) we have

$$\frac{dN_{2(1)}^{\text{opp}}}{dy_2} = N_0 \exp\left[-\tfrac{1}{4}(Bx_{T1}+\alpha) \frac{4Ap_{T2}^2}{4Ap_{T2}^2 + Bx_{T1} + \alpha} (y_2 - y_2^{\max}(x_{T1}, y_1))^2 \right], \qquad (3.3.1)$$

where

$$y_2^{\max}(x_{T1}, y_1) = \frac{\alpha}{Bx_{T1}+\alpha} y_1 + \frac{Bx_{T1}}{Bx_{T1}+\alpha} \bar{y}_1, \quad \bar{y}_1 = \tfrac{1}{2} \ln \frac{1 - \frac{1}{2} x_{T1} e^{y_1}}{1 - \frac{1}{2} x_{T1} e^{-y_1}}. \qquad (3.3.2)$$

The first remark we make is that y_2 distribution depends very weakly on A: one can safely take the limit $A \to \infty$, i. e. turn back to the zero width formula (1.1) without essential changes in (3.3.1). The p_{T2} dependence of the width Δy_2 is also very weak: even for $p_{T2} = 0.35$ GeV the width is greater than its asymptotic value $\Delta y_2^{\infty} = \frac{2}{\sqrt{Bx_{T1}+\alpha}}$ only by a factor 1.6, and for $p_{T2} > 0.5$ GeV the p_{T2} dependence of Δy_2 is completely negligible. On the other hand the width depends essentially on the value of α. It can be seen in Fig. 5,

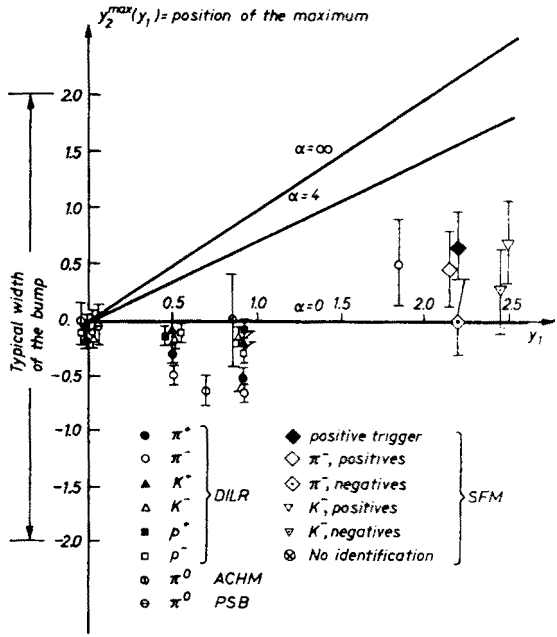

Fig. 6. Position of the maximum of the opposite side bump on y_2 axis as a function of the rapidity y_1 of the large p_T trigger. Data are taken from Refs [3–8]. Solid lines are the predictions of the model (Formula (3.3.2) with $\bar{y}_1$ neglected)

where the formula (3.3.1) is plotted. Thus, exactly as on the one-particle level, we conclude that only the model with $\alpha = 0$ is able to fit the large p_T data.

Let us come now to the problem of the position of maximum. The second term in (3.3.2) is consistent with zero in the present range of x_{T1}, y_1 and thus y_2^{max} depends essentially on the value of α.

To have the bump which stays at $y_2 = 0$ when y_1 changes from 0 to 2 once more the model with $\alpha = 0$ is needed.

3.4. p_{T1} dependence of the associated multiplicity

It is a well-known observation [3, 7, 5], that the associated multiplicity measured in the narrow bin in φ around $\varphi = \pi$ (i. e. exactly opposite to the trigger) grows nearly

linearly with p_1. From our formula (2.1.11) we find

$$\left.\frac{dN^{\text{opp}}_{\text{ch}(1)}}{d\varphi dy_2}\right|_{\substack{\varphi=\pi \\ y_2=0}} = \int_0^{p_{T1}} p_{T2}\,\frac{dN^{\text{opp}}_{\text{ch}(1)}}{\dfrac{d^3p_2}{E_2}}\,dp_{T2}$$

$$= \frac{\sqrt{A(Bx_{T1}+\alpha)}}{2\pi}\,p_{T1}\int_0^1 d\hat{x}_2\,\sqrt{\frac{4Ap_{T1}^2\hat{x}_2^2}{4Ap_{T1}^2\hat{x}_2^2+B\hat{x}_{T1}+\alpha}}\,F_{\text{ch}|J_2}(\hat{x}_2), \tag{3.4.1}$$

where we have changed the integration variable $p_{T2} \to \tilde{x}_2 = \dfrac{p_{T2}}{p_{T1}}$. Since $F_{\text{ch}|J_2}(\hat{x}_2)$ is finite for $\hat{x}_2 \to 0$, for sufficiently large p_{T1} we can replace the square root in the integrand by 1 and we obtain

$$\left.\frac{dN^{\text{opp}}_{\text{ch}(1)}}{d\varphi dy_2}\right|_{\substack{\varphi=\pi \\ y_2=0}} \approx \frac{\sqrt{A(Bx_{T1}+\alpha)}}{2\pi}\,p_{T1}\int_0^1 F_{\text{ch}|J_2}(\hat{x}_2)d\hat{x}_2 = \frac{1}{3\pi}\sqrt{A(Bx_{T1}+\alpha)}\,p_{T1}, \tag{3.4.2}$$

where the last equality follows from (3.1.1). Thus we obtain the effect observed experimentally.

As seen from the calculation presented above the growth of multiplicity exactly opposite to the trigger is of pure kinematical origin: it does not depend on the detailed

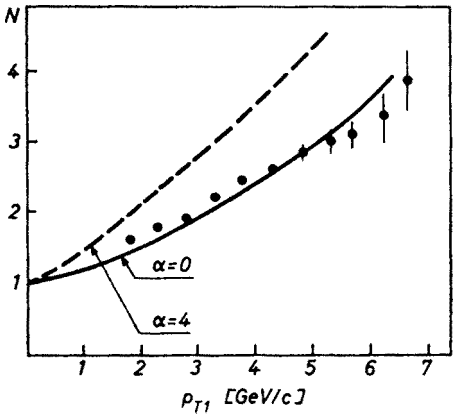

Fig. 7. Multiplicity of the charged particles in the angular region $|\varphi| < 23°$, $|y_2| < 1$ as a function of the transverse momentum of the trigger. Data are taken from Ref. [7], solid (dashed) line is the prediction of the model for $\alpha = 0$ ($\alpha = 4$) (formula (3.4.2) with the background (3.4.3))

shape of the jet structure function and therefore it would be present even for the jet with *constant* total multiplicity.

To compare the function (3.4.2) with the data, a low p_T background must be added to the jet contribution given by (3.4.2). Using the standard parametrization for low p_T

two-particle distribution we find

$$\left(\frac{dN_{\mathrm{ch}(1)}}{d\varphi dy_2}\right)_{\mathrm{low}\,P_T} \approx \frac{n_0}{2\pi}\,(1+ce^{-\frac{1}{\lambda}|y_1-y_2|}), \tag{3.4.3}$$

where the height of the rapidity plateau for charged particles $n_0 = 1.65$, the correlation coefficient $c = 0.75$, the correlation length $\lambda = 2$. Formula (3.4.2) with (3.4.3) added is compared with the CCR data [7] in Fig. 7.

Note that large value of α is once more excluded.

3.5. φ distribution

The azimuthal distribution of associated multiplicity was first measured by the PSB-Collaboration [3] and then by others groups. One observes a very broad enhancement on the opposite side to the large p_T particle. It can be seen in Fig. 8 where the φ distribution normalized to its low p_T value is presented for large p_T π^0 at 90°.

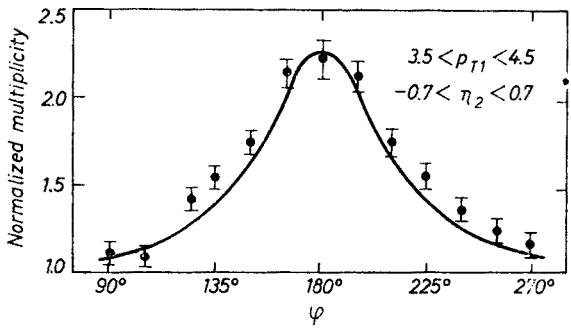

Fig. 8. Azimuthal distribution of associated charged particles. Data are taken from Ref. [3], the solid line is the prediction of the model (formula (3.5.1) with the background (3.5.7) and the low p_T distribution (3.5.8)

Integrating (2.1.11) over p_{T2} and neglecting the p_{T2} dependence of the square root factor $\sqrt{4Ap_{T2}^2/(4Ap_{T2}^2+Bx_{T1}+\alpha)}$ we find

$$\left.\frac{dN^{\mathrm{opp}}_{\mathrm{ch}(1)}}{d\varphi}\right|_{y_1=y_2=0} = \frac{1}{3\pi}\sqrt{A(Bx_{T1}+\alpha)}\;p_{T1}\Phi_{g_{\mathrm{ch}|J_2}}(\lambda), \tag{3.5.1}$$

where $\lambda = Ap_{T1}^2 \sin^2\varphi$ and

$$\Phi_{g_{\mathrm{ch}|J_2}}(\lambda) = (g_{\mathrm{ch}|J_2}+1)\int_0^1 e^{-\lambda x^2}(1-x)^{g_{\mathrm{ch}|J_2}}dx. \tag{3.5.2}$$

Note that for $\varphi = \pi$ we have $\lambda = 0$, $\Phi_{g_{\mathrm{sh}|J_2}}(0) = 1$ and (3.5.1) reduces to the formula (3.4.2) discussed in previous section. Thus the height of the Φ enhancement should grow with p_{T1}

according to the function presented in Fig. 7. The width of the bump is determined for the function (3.5.2). For small λ we have from (3.5.2)

$$\Phi_{g_{\mathrm{ch}|J_2}}(Ap_{T1}^2 \sin^2 \varphi) \approx \exp\left[-\frac{Ap_{T1}^2 \sin^2 \varphi}{(g_{\mathrm{ch}|J_2}+1)(g_{\mathrm{ch}|J_2}+2)}\right], \tag{3.5.3}$$

while for large λ

$$\Phi_{g_{\mathrm{ch}|J_2}}(Ap_{T1}^2 \sin^2 \varphi) \approx (g_{\mathrm{ch}|J_2}+1)\tfrac{1}{2}\sqrt{\pi}\,\frac{1}{\sqrt{A}\,p_{T1}|\sin\varphi|}. \tag{3.5.4}$$

As seen from (3.5.3), (3.5.4), the width of the φ distribution depends on the transverse momentum distribution (A dependence) as well as on the longitudinal structure function ($g_{\mathrm{ch}|J_2}$ dependence) in the jet fragmentation formula (1.5). In particular, for $g_{\mathrm{ch}|J_2} = 2$ we have

$$\Phi_2(\lambda) = \tfrac{3}{2}\left[\sqrt{\frac{\pi}{\lambda}}\left(1+\frac{1}{2\lambda}\right)\mathrm{erf}(\sqrt{\lambda}) + \frac{1}{\lambda}(e^{-\lambda}-2)\right]. \tag{3.5.5}$$

To compare (3.5.1) with the PSB data we must add low p_T background and divide the result by the low p_T distribution, i. e.

$$\left(\frac{dN}{d\varphi}\right)_{\mathrm{exp(PSB)}} = \frac{\left(\frac{dN}{d\varphi}\right)_{\mathrm{jet}} + \left(\frac{dN}{d\varphi}\right)_{\mathrm{background}}}{\left(\frac{dN}{d\varphi}\right)_{\mathrm{low}\ p_{T1}}}. \tag{3.5.6}$$

Jet component in (3.5.6) is given by (3.5.1) and for the background and low p_T component we take

$$\left(\frac{dN}{d\varphi}\right)_{\mathrm{background}} \approx \frac{n_0}{2\pi}, \tag{3.5.7}$$

$$\left(\frac{dN}{d\varphi}\right)_{\mathrm{low}\ p_{T1}} \approx \frac{n_0}{2\pi}(1+ce^{-\frac{1}{\lambda}|y_1-y_2|}). \tag{3.5.8}$$

The formula (3.5.8) is the usual low p_T parametrization. By taking the background as given by (3.5.7) we assume that soft secondaries accompanying the large p_T particle are produced by the same mechanism as in the usual low p_T events and are uncorrelated with the large p_T particle. Numerical values of n_0, c, λ we take, are given in the preceding section.

The formula (3.5.6) with (3.5.1), (3.5.5), (3.5.7), (3.5.8) included is compared with the data in Fig. 8.

3.6. Total associated multiplicity

As noted in Sec. 3.4, the linear growth of associated multiplicity exactly away to the large p_T trigger is only a kinematical effect and cannot provide any information about the true jet multiplicity.

To calculate the total jet multiplicity we have to integrate (2.1.11) over p_{T2}, y_2, φ. The result reads

$$N^{\text{opp}}_{\text{ch}(1)}(p_{T1}) = \tfrac{2}{3}(g_{\text{ch}|J_2}+1)\left[\ln\frac{p_{T1}}{m_\pi} + \sum_1^{g_{\text{ch}|J_2}} \frac{(-1)^k}{k}\binom{g_{\text{ch}|J_2}}{k} + O\left(\frac{m_\pi}{p_{T1}}\right)\right].$$

For $g_{\text{ch}|J_2} = 2$ we have

$$N^{\text{opp}}_{\text{ch}(1)}(p_{T1}) = 2\left[\ln\frac{p_{T1}}{m_\pi} - \tfrac{3}{2} + O\left(\frac{m_\pi}{p_{T1}}\right)\right]. \tag{3.6.1}$$

Note that the logarithmically increasing total jet multiplicity simply reflects our input for the jet fragmentation (1.6) with $\dfrac{dx}{x}$ (i. e. flat in rapidity) distribution in the small x region.

On the contrary to (1.2) and (1.4), here m_π appears as the mass scale. This is because the main contribution to $N^{\text{opp}}_{\text{ch}(1)}$ come from the soft particles for which the mass is a relevant parameter. In discussing the distributions (1.2) and (1.4) the masses can be neglected since

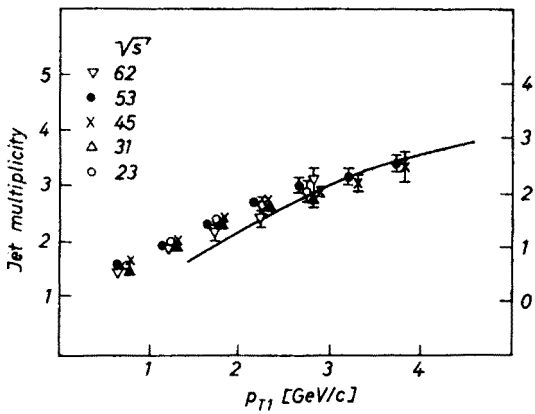

Fig. 9. Opposite side jet multiplicity, extracted from the charged multiplicity measurements by PSB Collaboration [3]. The right-hand scale correspond to the original PSB result, the left-hand includes the correction coming from the forward jet (Sec. 3.6). Solid line is the prediction of the model (formula (3.6.1)) — it refers to the left-hand scale

they refer to fast particles only. As seen from (3.6.1), for $p_{T1} = 3$ GeV/c, what is the typical value for the present correlation measurements, the opposite side jet contains in the mean 3 charged particles. It is a rather weak effect when compared with the total charge multiplicity in the ISR region $\langle n_{\text{ch}}\rangle = 12$ and thus the background analysis must be

performed especially carefuly. At this point it is more useful to subtract the background from the data instead of adding it to the formula (3.6.1), since we are interested just in the magnitude of the total *jet* multiplicity.

The analysis of this type was performed by the PSB-Collaboration [3]: jet multiplicity was calculated, roughly speaking, as a difference between the opposite side and the same side multiplicities associated with the large p_T π^0 at 90°. The resulting jet multiplicity is presented in Fig. 9 (right-hand scale). However, this procedure is correct only if the

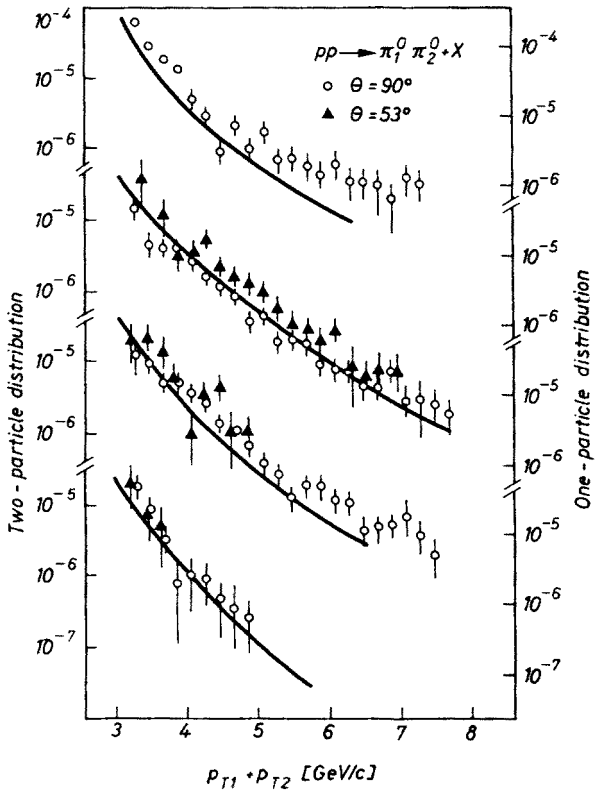

Fig. 10. Two-particle distribution for two large p_T in the same direction: $\theta_1 \approx \theta_2$, $\varphi \approx 0$ (left-hand scale). Solid lines are drawn by hand through the one-particle distribution data, taken for $p = p_1 + p_2$ (right-hand scale). Data from Ref. [2]

quasi-exclusive component gives the leading contribution to the same side correlations, i. e. the large p_T is produced always alone. From the ACHM data [2, 5] we know at present that this assumption is not true: we point out in Sec. 4.1, that to explain the same side correlations, a double-jet component must be present. Simultaneously, it gives only small correction to the opposite side correlations. It implies that the same side associated multiplicity contains except of the background also a part correlated with the large p_T particle (forward jet). It was found by the ACHM group, that after subtraction of the background it remains 0.85 ± 0.15 particles per event in the forward hemisphere more

exactly, in the angular sector: $|y_1-y_2|<1.5$, $|\varphi|<60°$. It is presented in Fig. 11 and discussed in Sec. 4.2. Thus to obtain the correct value of the opposite side jet multiplicity one has to *add* 0.85 ± 0.15 to the PSB result. We make it simply by shifting the scale: the left-hand scale in Fig. 9 refers to the corrected jet multiplicity. Solid line in Fig. 9 corresponds to the formula (3.6.1) – it refers to the left-hand scale too.

Let us note to the end of our analysis concerning the opposite side correlations that except of the P_{out} and x_E distributions where the values of A and $g_{\text{ch}|J_2}$ were fitted, all

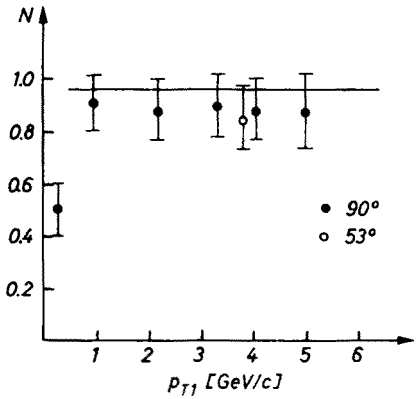

Fig. 11. Multiplicity of particles associated with the large p_{T1} particle measured in the angular region $|y_1-y_2|<1.5$, $|\varphi|<60°$ of the forward hemisphere versus the transverse momentum of the trigger. Data are taken from Ref. [5]. Solid line is the prediction of the model for large values of p_{T1} (formula (4.2.3))

other curves (Figs 5–9) were calculated without any further free parameters: B, α, N are fixed by the one-particle distribution, the overall normalization constant $n_{\text{ch}|J_2}$ is determined from (3.2), n_0, λ, c in (3.4.3) and (3.5.7), (3.5.8) are taken from low p_T physics.

4. Same side correlations — comparison with experiment

4.1. Two-particle inclusive distribution — momentum dependence and normalization

In the preceding Chapter we have found that the single-jet process with $A=2$, $\alpha=0, g_{2|J_2}=2$ can describe quite well the opposite side correlation data.

In the following we try to use the same process to calculate the same side correlations. We have two additional parameters in the formula (2.2.4), appearing in the two-particle jet distribution $n_{12|J_2}$, $g_{12|J_2}$. Using the phase space sum rule

$$\sum_2 \int_0^{1-\hat{x}_1} d\hat{x}_2 \hat{x}_2 G_{12|J_2}(\hat{x}_1, \hat{x}_2) = (1-\hat{x}_1) G_{1|J_1}(\hat{x}_1) \tag{4.1.1}$$

and retaining only the leading contribution on the left-hand side (i. e. the one with the smallest value of $g_{12|J_2}$) we find

$$g_{12|J_2} = g_{1|J_2}, \quad \sum_2 n_{12|J_2} = (g_{1|J_2}+1) n_{1|J_1}. \tag{4.1.2}$$

Let us look at the same side two-particle distribution when both particles are produced in the same direction, i. e. $\varphi \approx |y_1 - y_2| \approx 0$. We find from (2.2.4)

$$\left(\frac{d\sigma}{\frac{d^3p_1}{E_1}\frac{d^3p_2}{E_2}}\right)^{\text{same}}_{\varphi=|y_1-y_2|=0} = \frac{A}{\pi} r \frac{c_{12|J_2}}{(p_{T1}+p_{T2})^N} e^{-Bx_{T12}}. \tag{4.1.3}$$

The factor $r \equiv \frac{(p_{T1}+p_{T2})^2}{p_{T1}^2+p_{T2}^2}$ can be bounded $1 \leqslant r \leqslant 2$ and thus it gives only small variation of the total yield. In the following rough estimates we put it to be equal to 1.5. The remaining part of the formula (4.1.3) is nothing but the one-particle distribution taken for $p = p_1 + p_2$, the only difference being the overall normalization constant. This effect is indeed observed experimentally.

In Fig. 10 the two-particle data for two π°-s in the same direction are presented (left-hand scale). The solid lines are drawn by-hand through the one-particle data (right-hand scale). Both pieces of data are taken from ACHM experiment [2].

Thus it suffices to multiply the one-particle yield by a factor of 0.3 (see the difference between the left-hand and right-hand scales) in order to obtain the reasonable fit to the two-particle distribution for all typical ISR energies.

However, the problem arises if one looks at the normalization. Denoting

$$R_{12} = \frac{\left(E_1E_2\frac{d\sigma}{d^3p_1d^3p_2}\right)_{\varphi=|y_1-y_2|=0}}{\left(E\frac{d\sigma}{d^3p}\right)_{p=p_1+p_2}}$$

we have from (2.3.1), (2.3.5), (4.1.2)

$$R_{12} \approx \frac{A}{\pi} r \frac{c_{12|J_1}}{c_{1|J_1}} < \frac{A}{\pi} r\langle\hat{x}^{N-2}\rangle < 0.025$$

while the experimental value found in Fig. 8 reads

$$R_{12} = 0.30.$$

At this point our model fails: the quasi-exclusive contribution gives 10 times too small value of the same side correlations. The reason is quite obvious: in the single-jet process it is much easier to produce one large p_T particle than a pair of them since the single particle can be the jet particle while the pair in the same side can be produced only as a result of jet J_2 fragmentation. But, as noted in Section 2.3, the jet fragmentation introduces the damping factor $\langle\hat{x}^{N-2}\rangle$ relative to the quasi-exclusive production and therefore the ratio R_{12} is very small.

The situation is quite different for the double jet process: now the single particle as well as the pair are produced by the jet fragmentation and the damping factors $\langle \hat{x}^{N-2} \rangle$ *cancel* in calculating of R_{12}; we find

$$R_{12} \approx \frac{A}{\pi} r \frac{c_{12|J_1}}{c_{1|J_1}} \approx \frac{A}{\pi} r = 1.26.$$

Hence R_{12} is too small by a factor of 10 for the single-jet process and too large by a factor of 4 for the double-jet process.

The simplest guess one can make to solve the problem is that both types of processes contribute. Let us try to calculate R_{12} in this case. We have

$$R_{12} = \frac{A}{\pi} r \frac{c^{S}_{12|J_1} + c^{D}_{12|J_1}}{c^{S}_{1|J_1} + c^{D}_{1|J_1}} = \frac{A}{\pi} r \frac{\langle \hat{x}^{N-2} \rangle + R^{I}_{DS}}{1 + R^{I}_{DS}} \approx \frac{A}{\pi} r \frac{R^{I}_{DS}}{1 + R^{I}_{DS}},$$

where

$$R^{I}_{DS} = \frac{c^{D}_{12|J_1}}{c^{S}_{1|J_1}} = \langle \hat{x}^{N-2} \rangle \frac{c^{D}_{J_1}}{c^{S}_{J_1}} \equiv \langle \hat{x}^{N-2} \rangle R^{E}_{DS}.$$

To reproduce the experimental value $R_{12} = 0.3$ one must take

$$R^{I}_{DS} = 0.31$$

what in turn gives

$$R^{E}_{DS} = \frac{0.31}{\langle \hat{x}^{N-2} \rangle} > 17.$$

The meaning of the ratios R^{E}_{DS} and R^{I}_{DS} is the following: R^{E}_{DS} is the ratio of the hard scattering cross-sections in the double jet and single jet processes; R^{I}_{DS} measures the relative contributions of the double- and single-jet processes to the one-particle inclusive distribution and to the two-particle distribution on the opposite side, since

$$c_{1|J_1} = c^{S}_{J_1} + c^{D}_{1|J_1} = c^{S}_{J_1} + \langle \hat{x}^{N-2} \rangle c^{D}_{J_1} = c^{S}_{J_1}(1 + R^{I}_{DS}).$$

Thus the correction from the double-jet process to the opposite side correlations is only of order of 30%: the quasi-exclusive contribution dominates (70%) and our results found in the preceding Chapter remain valid to a good approximation.

Let us summarize the results of this section:

1. The single-jet component is not able to reproduce the large value of the same side correlations: it fails by a factor of 10.

2. The correct value of R_{12} can be obtained by adding the double-jet component with the hard scattering cross-section greater at least by a factor of 17 than the corresponding cross-section for the single jet component.

3. The double-jet component gives more than 90% of the two-particle distribution on the same side.

4. The single jet component gives about 70% of the one particle distribution and of the two-particle distribution on the opposite side.

To the end of this Section we wish to note that the problem discussed above was considered recently in a slightly more phenomenological context (i. e. without refering to hard scattering models) by S. D. Ellis et al. in [10]. One can easily verify that the parameter α_h introduced in [10] is nothing but $1/R_{DS}^{I}$ in our language. The value $\alpha_h = 4$ obtained in [10] can be compared with $1/R_{DS}^{I} = 3.2$, found by means of the rough estimates, presented above.

4.2. Momentum dependence of the associated multiplicity

The experimental information is here very simple: the multiplicity of particles produced in the same side as the large p_T trigger does not depend on p_{T1} and is of order of 1 after subtraction of the background (see Fig. 11 where the ACHM data [5] in the angular region: $|y_1 - y_2| < 1.5$, $|\varphi| < 60°$ are presented. The same side multiplicity was also measured by PSB [3], CCR [7] and DILR [4] groups. The ACHM data are most useful for our purposes due to the background subtraction).

From (2.2.4) we find

$$N_{ch(1)}^{same}(p_{T1}) \approx \frac{c_{12|J_1}}{c_{1|J_1}} \int \frac{dp_{T2}}{m_{T2}} \left(\frac{p_{T1}}{p_{T1}+p_{T2}}\right)^N e^{-Bx_{T2}} \xrightarrow[\text{large } p_{T1}]{}$$

$$\frac{c_{12|J_1}}{c_{1|J_1}} \int_0^\infty \frac{dp_{T2}}{\sqrt{p_{T2}^2+m^2}} e^{-Bx_{T2}} = 0.23 \frac{c_{12|J_1}}{c_{1|J_1}}, \tag{4.2.1}$$

where the last integral is calculated for $m = m_\pi$, $B = 13$. Thus we obtain indeed the constant multiplicity (at least for large values of p_{T1}) and using the experimental value of R_{12} (see Sec. 4.1) we get

$$N_{ch(1)}^{same} = 0.23 \frac{\pi}{Ar} 2R_{12} = 1.07. \tag{4.2.2}$$

The factor of 2 is present since we ask about the charged multiplicity and have to our disposal the value of R_{12} for two π^0-s.

It is interesting to note, that the same side multiplicity tends to some constant with p_{T1} increasing in any fixed angular region (and not only when integrated over the all forward hemisphere). We have from (2.2.4)

$$N_{ch(1)}^{same}|_{|y_1-y_2|<y_0, |\varphi|<\varphi_0} \xrightarrow[\text{large } p_{T1}]{} \text{erf}(\sqrt{A}|\sin\varphi_0|)\,\text{erf}(\sqrt{A}\,y_0) N_{ch(1)}^{same}. \tag{4.2.3}$$

In particular, the ACHM data presented in Fig. 11 correspond to $y_0 = 1.5$, $\varphi_0 = 60°$. From (4.2.3) we obtain

$$N_{ch(1)}^{same}|_{|y_1-y_2|<1.5, |\varphi|<60°} \approx 0.96,$$

what is consistent with the experimental value 0.85 ± 0.15.

4.3. y_2 dependence

Contrary to the broad bump on the opposite side, the same side rapidity distribution is narrow, centred at the rapidity of the trigger and shrinks prominently with increasing momentum of the associated particles. All these effects are typical for the jet dynamics and are certainly present in our formula (2.2.4). We have

$$\frac{dN_{2(1)}^{\text{same}}}{dy_2} = N_0 e^{-A\frac{p_{T1}^2 p_{T2}^2}{p_{T1}^2+p_{T2}^2}(y_1-y_2)^2}. \tag{4.3.1}$$

The function (4.3.1) with $A = 2$ is compared with the ACHM data [8] in Fig. 12.

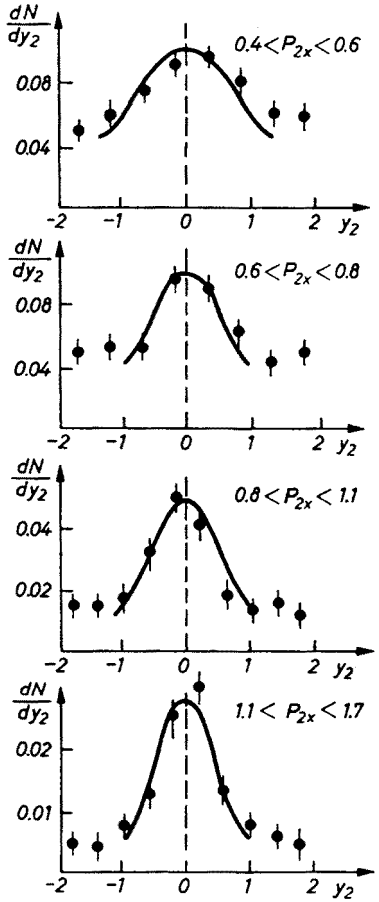

Fig. 12. y_2 distribution of the same side associated multiplicity. Solid lines are the predictions of the model (formula (4.3.1)). No background corrections are made and therefore N_0 in (4.3.1) is fitted to each curve separately. Data from Ref. [8]

The essential difference between y_2 shapes on the same and opposite sides find in the parton models a very convincing explanation: since jets are colimated, the direction of the triggered large p_T particle fixes approximately the direction of the forward jet and we observe a narrow bump in y_2 around y_1. On the other hand, in the same measurement the

direction of the opposite side jet is not fixed because the c_1c_2 system has some finite Y distribution. The width of the opposite side y_2 distribution is determined by the width of the Y distribution of c_1c_2 system, since

$$y_2 = Y+\hat{y}_2 \approx Y+\hat{y}_{J_2} = Y-\hat{y}_{J_1} \approx Y-y_1,$$

$$\Delta y_2 \approx \Delta Y = \frac{2}{\sqrt{Bx_{T1}+\alpha}}. \tag{4.3.2}$$

Thus the same side y_2 distribution measures the width of the jet, while the opposite side y_2 distribution measures the mobility of the c_1c_2 system on the rapidity axis.

5. *Summary*

We end this paper with a brief review of the results we have obtained.

We have analysed the large p_T data using general parton model formulas and we have found in this way some non-trivial constraints which must be obeyed by the "good" parton model.

1) Strong evidence is found for a very special form of the hard scattering cross-section, reported first in [9]: $\frac{d\sigma_H}{d\hat{t}}$ should be only a function of $\hat{p}_T$, i. e. it should be independent of angle at fixed $\hat{p}_T$.

2) It is proved that the same side correlation data cannot be explained by means of one leading subprocess: the single jet process gives much too small, and double-jet process much too large value of the correlations.

One can obtain the correct description of correlations by adding both contributions but only if the double-jet component has the hard scattering cross-section larger at least by a factor of 17 than the single-jet component.

Double-jet component dominates in the same side correlations (90%) and the single-jet process gives the leading contribution (70%) to the opposite side correlations.

3) The jets in the final state should be rather broad with the mean transverse momentum of the order of 0.63 GeV.

4) The jet structure function should fall for $x \to 1$ like $(1-x)^2$.

The models which posses all these properties give good description of existing large p_T data on the two-particle level.

The authors are grateful to A. Białas and to R. Wit for continuous help and encouragement during the course of this work and for the critical reading of the manuscript.

APPENDIX

In this Appendix we calculate formulas (2.1.3) and (2.2.4) for the two-particle distribution.

Let us start with the opposite side distribution. To perform the integration over angles in (2.1.1) we approximate the exponents in (1.5) using the steepest descend method.

We find

$$e^{-A(\hat{p}_{T1|J_1}{}^2+\hat{p}_{T2|J_2}{}^2)} \approx e^{-A\frac{p_{T1}{}^2 p_{T2}{}^2}{p_{T1}{}^2+p_{T2}{}^2}[\sin^2\varphi+(2Y-(y_1+y_2))^2]}$$

$$\times e^{-A(p_{T1}{}^2+p_{T2}{}^2)\left\{\left[\hat{\varphi}_{1|J_1}{}^2+\frac{p_{T2}{}^2}{p_{T1}{}^2+p_{T2}{}^2}(\varphi-\pi)^2\right]+[\hat{y}_{J_1}-\frac{1}{2}(y_1-y_2)]^2\right\}}.$$

Denoting $\hat{x}_1 = \dfrac{\hat{p}_1}{\hat{p}_{J_1}} \approx \dfrac{p_{T1}}{p_{TJ_1}}$, $\hat{x}_2 = \dfrac{\hat{p}_2}{\hat{p}_{J_2}} \approx \dfrac{p_{T2}}{p_{TJ_2}}$ we obtain

$$\left(\frac{d\sigma}{\frac{d^3p_1}{E_1}\frac{d^3p_2}{E_2}}\right)_{c_1c_2\to J_1J_2} = \frac{A}{\pi}\frac{p_{T1}^2 p_{T2}^2}{p_{T1}^2+p_{T2}^2} e^{-A\frac{p_{T1}{}^2 p_{T2}{}^2}{p_{T1}{}^2+p_{T2}{}^2}[\sin^2\varphi+(2Y-(y_1+y_2))^2]}$$

$$\times \int_{x_{T1}}^{1}\frac{d\hat{x}_1}{\hat{x}_1^3}\int_{x_{T2}}^{1}\frac{d\hat{x}_2}{\hat{x}_2^3}\tfrac{1}{2}\left(\frac{\hat{x}_1}{p_{T1}}+\frac{\hat{x}_2}{p_{T2}}\right)\delta\left(\frac{p_{T1}}{\hat{x}_1}-\frac{p_{T2}}{\hat{x}_2}\right)F_{1|J_1}(\hat{x}_1)$$

$$F_{2|J_2}(\hat{x}_2)\frac{\hat{s}}{\pi}\frac{d\sigma_H}{dt}\delta(\hat{s}+\hat{t}+\hat{u})$$

The integration over x_{c_1}, x_{c_2} in (2.5) can be performed by the method described in Ref. [9]: we change variables x_{c_1}, $x_{c_2} \to M$, Y, where M and Y are the mass and rapidity of the c_1c_2 system and approximate the Y dependence of the integrand by a Gaussian. Using the parametrization (2.4) for the hard scattering cross-section we obtain finally

$$\left(\frac{d\sigma}{\frac{d^3p_1}{E_1}\frac{d^3p_2}{E_2}}\right)_{AB\to 1+2+X} = \frac{A}{\pi}\frac{p_{T1}^2 p_{T2}^2}{p_{T1}^2+p_{T2}^2} e^{-A\frac{p_{T1}{}^2 p_{T2}{}^2}{p_{T1}{}^2+p_{T2}{}^2}\sin^2\varphi}$$

$$\times \frac{c_0 n_{c_1|A} n_{c_2|B} H(1)}{4^N}\int_{x_{T1}}^{1}\frac{d\hat{x}_1}{\hat{x}_1^3}\int_{x_{T2}}^{1}\frac{d\hat{x}_2}{\hat{x}_2^3}\tfrac{1}{2}\left(\frac{\hat{x}_1}{p_{T1}}+\frac{\hat{x}_2}{p_{T2}}\right)$$

$$\times\delta\left(\frac{p_{T1}}{x_1}-\frac{p_{T2}}{x_2}\right)F_{1|J_1}(\hat{x}_1)F_{2|J_2}(\hat{x}_2)\frac{1}{p_{TJ_1}^N}\frac{e^{-b(x_{TJ_1},y_1)x_{TJ_1}}}{\sqrt{bx_{TJ_1}+\alpha+4A\dfrac{p_{T1}^2p_{T2}^2}{p_{T1}^2+p_{T2}^2}}}$$

$$\times e^{-\frac{1}{4}(bx_{TJ_1}+\alpha)\frac{4A\frac{p_{T1}{}^2p_{T2}{}^2}{p_{T1}{}^2+p_{T2}{}^2}}{bx_{TJ_1}+\alpha+4A\frac{p_{T1}{}^2p_{T2}{}^2}{p_{T1}{}^2+p_{T2}{}^2}}(y_2-\tilde{y}_2^{\max}(x_{TJ_1},y_1))^2} \qquad \text{(A.1)}$$

where $b = g_{c_1|A} + g_{c_2|B}$,

$$b(x_{TJ_1}, y_1) = b\left[\frac{bx_{TJ_1}}{bx_{TJ_1}+\alpha}\,\tfrac{1}{2}(1+\cosh y_1) + \frac{\alpha}{bx_{TJ_1}+\alpha}\cosh y_1\right],$$

$$\tilde{y}_2^{\max}(x_{TJ_1}, y_1) = \frac{\alpha}{bx_{TJ_1}+\alpha}\,y_1 + \frac{bx_{TJ_1}}{bx_{TJ_1}+\alpha}\,\bar{y}_1,$$

$$\bar{y}_1 = \tfrac{1}{2}\ln\frac{1-\frac{1}{2}x_{TJ_1}e^{y_1}}{1-\frac{1}{2}x_{TJ_1}e^{-y_1}}. \tag{A.1'}$$

The last step is to perform integrations over $\hat{x}_1$, $\hat{x}_2$ in (A.1). It can be done by using the mean value theorem (see Ref. [9]). It is convenient to consider separately the cases $x_{T1} \geqslant x_{T2}$, $x_{T1} < x_{T2}$. For $x_{Ti} > x_{Tk}$, $(i, k) = (1, 2)$ or $(2, 1)$, we perform the x_{Tk} integration with the δ function and x_{Ti} integration by means of the mean value theorem.

The final result can be expressed as follows: denoting by

$$\begin{aligned}\varrho_2(p_{T1}, p_{T2}, y_1, y_2, \varphi; 1|J_1, 2|J_2) &= \frac{c_{1|J_1}}{p_{T1}^N}\,e^{-B(x_{T1},y_1)x_{T1}}\,\frac{1}{p_{T2}^2+\mu^2}\,F_{2|J_2}\left(\langle\hat{x}_1\rangle\frac{p_{T2}}{p_{T1}}\right)\\ \times\frac{\exp\left[-\left(\frac{\sin\varphi}{\Delta\varphi}\right)^2\right]}{\sqrt{\pi}\,\Delta\varphi}&\frac{\exp\left[-\left(\frac{y_2-\tilde{y}_2^{\max}(x_{T1},y_1)}{\Delta y_2}\right)^2\right]}{\sqrt{\pi}\,\Delta y_2},\end{aligned} \tag{A.2}$$

where $N = 2n$,

$$B(x_{T1}, y_1) = \frac{1}{\langle\hat{x}_1\rangle}\,b\left(\frac{x_{T1}}{\langle\hat{x}_1\rangle},\ y_1\right), \qquad B \equiv B(x_{T1}, 0) = B(0, 0),$$

$$\langle\hat{x}_1\rangle = \frac{N-3}{N-2+g_{1|J_1}}$$

$$c_{1|J_1} = \langle\hat{x}_1^{N-2}\rangle c_{J_1}, \qquad \langle\hat{x}_1^{N-2}\rangle = \int_0^1 d\hat{x}_1\hat{x}_1^{N-2}G_{1|J_1}(\hat{x}_1),$$

$$c_{J_1} = \frac{c_0}{4^N}\,H(1)\,\frac{n_{c_1|A}n_{c_2|B}}{\sqrt{Bx_{T1}+\alpha}}, \qquad \Delta\varphi = \frac{1}{\sqrt{A}}\,\frac{\sqrt{p_{T1}^2+p_{T2}^2}}{p_{T1}p_{T2}},$$

$$\Delta y_2 = \frac{2}{\sqrt{Bx_{T1}+\alpha}}\sqrt{\frac{4A\frac{p_{T1}^2p_{T2}^2}{p_{T1}^2+p_{T2}^2}+Bx_{T1}+\alpha}{4A\frac{p_{T1}^2p_{T2}^2}{p_{T1}^2+p_{T2}^2}}},$$

$$y_2^{\max}(x_{T1}, y_1) = \tilde{y}_2^{\max}\left(\frac{x_{T1}}{\langle x_1\rangle},\ y_1\right)$$

we can write for the process $(A, B) \to (c_1 c_2) \to (J_1 J_2 \to (1, 2) + X$

$$\left(\frac{d\sigma}{\frac{d^3p_1}{E_1}\frac{d^3p_2}{E_2}}\right)_{AB\to 1+2+X}$$

$$= \varrho_2(p_{T1}, p_{T2}, y_1, y_2, \varphi; 1|J_1, 2|J_2)\theta(p_{T1} - p_{T2})$$

$$+ \varrho_2(p_{T2}, p_{T1}, y_1, y_2, \varphi; 2|J_2, 1|J_1)\theta(p_{T2} - p_{T1})$$

$$+ \varrho_2(p_{T1}, p_{T2}, y_1, y_2, \varphi; 1|J_2, 2|J_1)\theta(p_{T1} - p_{T2})$$

$$+ \varrho_2(p_{T2}, p_{T1}, y_1, y_2, \varphi; 2|J_1, 1|J_2)\theta(p_{T2} - p_{T1}). \tag{A.3}$$

The last two terms have appeared as a result of the symmetrization $J_1 \leftrightarrow J_2$. For the quasi-exclusive contribution ($1 = J_1$) one has to put in (A.2)

$$\langle \hat{x}_1 \rangle = \langle \hat{x}_1^{N-2} \rangle = 1$$

$$\Delta\varphi = \frac{1}{\sqrt{A}}\frac{1}{p_{T2}},$$

$$\Delta y = \frac{2}{\sqrt{Bx_{T1} + \alpha}}\sqrt{\frac{4Ap_{T2}^2 + Bx_{T1} + \alpha}{4Ap_{T2}^2}}.$$

To give some feeling about the relative importance of various terms appearing in (A.3) we note that:

a) the second and the fourth term are damped relative to the first and to the third, respectively, by the factor $\left(\frac{p_{T1}}{p_{T2}}\right)^{N-2}$;

b) if $J_1 = J_2$, the symmetrization $J_1 \leftrightarrow J_2$, resulting in the last two terms, reduces to multiplication ot the first two terms by a factor of 2. If $J_1 \neq J_2$, the normalization factors $c_{1|J_2}, c_{1|J_2}$ differ very essentially ($\langle \hat{x}_1^{N-2} \rangle$ is rapidly varying function of $g_{1|J_{1,2}}$ and to a first approximation we can retain only the contribution with the smaller value of g).

If we fix labeling of jets in such a manner that $g_{1|J_1} \leqslant g_{1|J_2}$ then, taking a) and b) into account, the leading contribution in (A.3) can be displayed as follows:

$$\left(\frac{d\sigma}{\frac{d^3p_1}{E_1}\frac{d^3p_2}{E_2}}\right)_{AB\to 1+2+X}$$

$$= (1 + \delta_{g_1|J_1, g_1|J_2})\left[\theta(x_{T1} - x_{T2}) + O\left(\left(\frac{x_{T1}}{x_{T2}}\right)^{N-2}\right)\theta(x_{T2} - x_{T1})\right]$$

$$\times \varrho_2(p_{T1}, p_{T2}, y_1, y_2, \varphi; 1|J_1, 2|J_2),$$

where ϱ_2 is given by (A.2).

The same side two-particle distribution can be calculated by the same method. We have

$$e^{-A(\hat{p}_{T1|J_1}^2+\hat{p}_{T2|J_2}^2)} \approx e^{-A(p_{T1}^2+p_{T2}^2)\left(\hat{\varphi}_{1|J_1}+\frac{p_{T2}^2}{p_{T1}^2+p_{T2}^2}\varphi\right)^2}$$

$$\times e^{-A(p_{T1}^2+p_{T2}^2)\left(\hat{y}_{J_1}-\hat{y}_1-\frac{p_{T2}^2}{p_{T1}^2+p_{T2}^2}(y_1-y_2)\right)^2} e^{-A\frac{p_{T1}^2 p_{T2}^2}{p_{T1}^2+p_{T2}^2}[\sin^2\varphi+(y_1-y_2)^2]}$$

Integration over angles in (2.1.1) gives

$$\left(\frac{d\sigma}{\frac{d^3p_1}{E_1}\frac{d^3p_2}{E_2}}\right)_{c_1c_2\to 1+2+X}$$

$$= \frac{A}{\pi}\frac{(p_{T1}+p_{T2})^2}{p_{T1}^2+p_{T2}^2} e^{-A\frac{p_{T1}^2 p_{T2}^2}{p_{T1}^2+p_{T2}^2}[\sin^2\varphi+(y_1-y_2)^2]}$$

$$\times \int_{x_{T12}}^{1} \frac{d\hat{x}_{12}}{\hat{x}_{12}^3} F_{12|J_1}(\hat{x}_{12}) \frac{\hat{s}}{\pi}\frac{d\sigma_H}{d\hat{t}}\,\delta(\hat{s}+\hat{t}+\hat{u}),$$

where $\hat{x}_{12} = \hat{x}_1+\hat{x}_2$, $x_{T12} = x_{T1}+x_{T2}$.

Integrating over Y and x_{12} exactly as in Ref. [9] we obtain finally the formula (2.2.4).

REFERENCES

[1] P. Darriulat et al., *An Inclusive Measurement of Charged Particles Accompanying a High Transverse Momentum π^0 at the ISR Split Field Magnet Facility*, Contribution G5–21 to the International Conference on High Energy Physics, Palermo (Italy), 23–28 June 1975.

[2] K. Eggert et al., *Nucl. Phys.* **B98**, 73 (1975).

[3] G. Finocchiaro et al., *Phys. Lett.* **50B**, 396 (1974).

[4] DILR Collaboration — results presented by S. Rock during the ISR Discussion Meeting Nr 13, February 1975, CERN Report.

[5] K. Eggert et at., *Nucl. Phys.* **B98**, 93 (1975).

[6] M. Della Negra et al., *Study of Events with a Positive Particle of Large Transverse Momentum Emitted near the Forward Direction in pp Collisions at $\sqrt{s} = 52.5$ GeV*, CERN/D. Ph. II/PHYS 75–32 Rev., June 1975.

[7] F. W. Büsser et al., *Phys. Lett.* **51B**, 306 (1974).

[8] *Correlations among Large P_T Particles*, CERN report 17 from the ISR Discussion Meeting, November 1975 — results from the CERN-412 Collaboration (SFM and external lead glass detector) presented by J. Strauss.

[9] W. Furmański, J. Wosiek, *Acta Phys. Pol.* **B8**, 633 (1977).

[10] S. D. Ellis, M. Jacob, P. V. Landshoff, *Jets and Correlations in Large p_T Reactions*, CERN preprint TH. 2109, December 1975.